Localized ductile shear below the seismogenic zone: Structural analysis of an exhumed strike-slip fault, Austrian Alps

Joshua Cole,[1] Bradley Hacker,[1] Lothar Ratschbacher,[2] James Dolan,[3] Gareth Seward,[1] Erik Frost,[3] and Wolfgang Frank[4]

Received 5 February 2007; revised 21 May 2007; accepted 11 September 2007; published 14 December 2007.

[1] The Miocene Salzachtal-Ennstal-Mariazell-Puchberg (SEMP) strike-slip fault in Austria allows study of the internal structure of a fault zone from the near surface to ~30 km depth. As it enters the Tauern Window along the Rinderkarsee shear zone, the SEMP fault passes from a dominantly brittle to a dominantly ductile structure. The shear zone consists of three 1- to 100-m-wide zones of brittle-ductile and ductile deformation separated by 500-m-wide zones of less deformed rocks. The southern shear zone is mylonitic, with ductile amphibole and plagioclase; weak crystal preferred orientations imply that the main deformation mechanism was dislocation-accommodated grain boundary sliding. The northern and central shear zones are characterized by discrete millimeter-wide shear zones with ductile quartz, muscovite, and biotite and brittle feldspar. Shear zone nucleation at the grain scale involved dislocation creep and the transformation of plagioclase to muscovite; strain then localized in muscovite-rich grain boundary shear zones that linked to form throughgoing shear zones.

Citation: Cole, J., B. Hacker, L. Ratschbacher, J. Dolan, G. Seward, E. Frost, and W. Frank (2007), Localized ductile shear below the seismogenic zone: Structural analysis of an exhumed strike-slip fault, Austrian Alps, *J. Geophys. Res.*, *112*, B12304, doi:10.1029/2007JB004975.

1. Introduction

[2] Fault mechanics and earthquake rupture and termination processes are inexorably linked to the physical properties of fault zones. The brittle-ductile transition plays a key role in all these processes, such that understanding active deformation mechanisms at midcrustal depths is a critical component to our understanding of earthquake physics.

[3] In the early 1980s a paradigm for crustal rheology was developed that considered the crust to be composed of two distinct layers: a seismogenic upper crust deforming via pressure-dependent/temperature-insensitive brittle frictional sliding, and an aseismic lower crust deforming via temperature-dependent/pressure-insensitive ductile processes such as dislocation creep and diffusion creep [*Brace and Kohlstedt*, 1980; *Sibson*, 1982]. This idea gained credibility because the predicted crossover from frictional sliding to creep derived from extrapolation of laboratory constitutive relations for quartzofeldspathic crust is ~10–15 km deep, a depth that accords with observed seismicity [*Meissner and Strehlau*, 1982; *Ito*, 1999]. This paradigm continues to serve as the basis for modern geodynamic models [e.g., *Ellis and Stöckhert*, 2004] and interpretations of the strength of the crust [*Jackson et al.*, 2004].

[4] Studies of exhumed faults and experimentally deformed samples show, however, that the transition from brittle faulting to ductile creep is not discrete but is a zone in which deformation mechanisms and strain localization depend on pressure, temperature, strain rate, grain size, fluid activities, mineralogy, phase transformations, and microstructure [e.g., *Tullis and Yund*, 1977; *Carter and Kirby*, 1978; *Sibson*, 1980; *Passchier*, 1982; *Sibson*, 1982; *Hobbs et al.*, 1986; *Rutter*, 1986; *Janecke and Evans*, 1988; *Scholz*, 1988; *Shimamoto*, 1989; *Hacker and Christie*, 1990; *Tullis and Yund*, 1992; *Chester*, 1995; *White*, 1996; *Hacker*, 1997; *Shigematsu et al.*, 2004; *Lin et al.*, 2005]. In the current view [e.g., *Scholz*, 2002], summarized by Figure 1, the upper part of the brittle-ductile transition is characterized by ductile flow of quartz and brittle flow of feldspar during interseismic cycles and by coseismic brittle failure of all minerals whenever an earthquake generated at shallower depth propagates downward into the transition. The lower part of the brittle-ductile transition is considered to be characterized by ductile flow of quartz and brittle flow of feldspar and no coseismic deformation. Beneath the brittle-ductile transition, quartz and feldspar are both ductile.

[5] For an improved understanding of the brittle-ductile transition and earthquake physics, it is important to know how accurately this paradigm describes the Earth and in what major ways the different variables listed above interact to influence seismic and interseismic processes. This paper addresses several specific questions of interest in this

[1] Earth Sciences, University of California, Santa Barbara, California, USA.
[2] Geowissenschaften, Technische Universität Bergakademie Freiberg, Freiberg, Germany.
[3] Earth Sciences, University of Southern California, Los Angeles, California, USA.
[4] Cryptographic Equipment Assessment Laboratory, Slovak Academy of Sciences, Bratislava, Slovakia.

0148-0227/07/2007JB004975$09.00

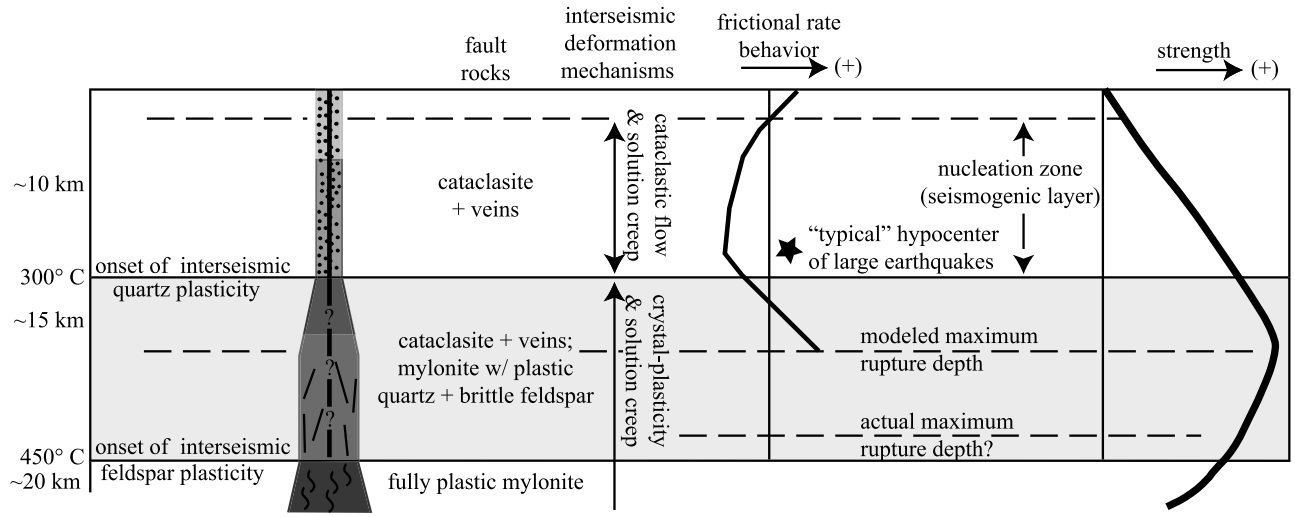

Figure 1. Generalized shear zone model after *Scholz* [1988] and *Chester* [1995]. The brittle-ductile transition (grey layer) is defined as occurring between quartz plasticity and feldspar plasticity for quartzofeldspathic rock. Seismic behavior is defined by a friction rate parameter [*Ruina*, 1983]: if negative, friction is velocity weakening and unstable (stick-slip); if positive, friction is velocity strengthening and stable (creep). Cataclastic flow, solution transfer creep, and dislocation creep are velocity strengthening [*Chester*, 1995], whereas localized slip is rate weakening and predicted to be active under higher shear strain and intermediate temperatures. Our findings indicate that fluid-driven reactions within the brittle-ductile transition can drive transformational plasticity in feldspars at anomalously low temperature ($\ll$500°C) and may make feldspars weaker than quartz in fault zones. In addition, the presence of localized ductile shear zones within the brittle-ductile transition indicates that ductile shear zones may underlie brittle strike-slip faults.

regard. (1) How does strain partitioning change with depth across the brittle-ductile transition; is there a single fault/shear zone that simply gets progressively wider with depth? (2) How do deformation mechanisms change across the brittle-ductile transition; how common is the combination of quartz crystal plasticity, feldspar brittle failure and solution transfer creep? (3) By what means can transformational softening affect the rheology of Earth materials within the brittle-ductile transition?

[6] This study focuses on these questions through macroscopic to microstructural observations of the Miocene strike-slip Salzachtal-Ennstal-Mariazell-Puchberg (SEMP) fault in central and eastern Austria. The SEMP fault has been differentially exhumed along strike, allowing one to study the detailed structure of the fault rocks from the Earth's surface down to ~30 km depth, simply by moving along strike from the Vienna basin to the Tauern Window (Figure 2). Coincident with its entry into the Tauern Window, the SEMP fault passes from a dominantly brittle to a dominantly ductile structure. The Tauern segment of the SEMP fault therefore represents a key location for studying earthquake nucleation and midcrustal rheology.

2. Geologic Setting

[7] The ENE striking SEMP fault of the Austrian Alps is a continuous 400-km-long sinistral strike-slip zone with ~60 km of late Oligocene-Miocene displacement across its western end (the Salzachtal fault; Figure 2) [*Ratschbacher et al.*, 1991a, 1991b; *Peresson and Decker*, 1997a; *Linzer et al.*, 2002]. The SEMP cuts through the tectonostratigraphy typical of this part of the Alpine orogen, European continental crust (Lower Schieferhülle and Zentralgneis), Penninic oceanic rocks and flysch (Upper Schieferhülle), and Austroalpine (Adriatic plate) continental crust [e.g., *Linzer et al.*, 2002]. It was activated during collision between the Adriatic and European plates, either as a result of eastward lateral extrusion [*Ratschbacher et al.*, 1991a, 1991b; *Frisch et al.*, 1998; *Linzer et al.*, 2002] or oblique indentation by the South Alpine block [*Rosenberg et al.*, 2004].

[8] Late in the lateral extrusion process, a series of SEMP-related ductile shear zones propagated down into the Tauern Window [e.g., *Behrmann and Frisch*, 1990; *Ratschbacher et al.*, 1991a; *Linzer et al.*, 2002]. Of these, the Greiner shear zone shows that deformation was active during decompression from 8–10 kbar and 450–550°C to 6–8 kbar and 500–570°C [*Selverstone et al.*, 1984; *Behrmann and Frisch*, 1990; *Selverstone et al.*, 1991]. The Tauern Window was exhumed by approximately N-S shortening: rising from ~25 km depth at 30 Ma, to ~10–15 km at 25–17 Ma, and to ~4 km by 7 Ma [*Oxburgh et al.*, 1966; *Cliff et al.*, 1985; *Spear and Franz*, 1986; *von Blanckenburg et al.*, 1989; *Christensen et al.*, 1994]. It is the difference between the Tertiary N-S shortening across the Tauern Window (>50% or ~150 km) [*Ratschbacher et al.*, 1991a] and the much smaller magnitude of shortening (<30% or ~70 km) in the Vienna basin that produced the differential exhumation of the SEMP.

[9] There is little modern geochronology that dates displacement along the SEMP and its continuation into the

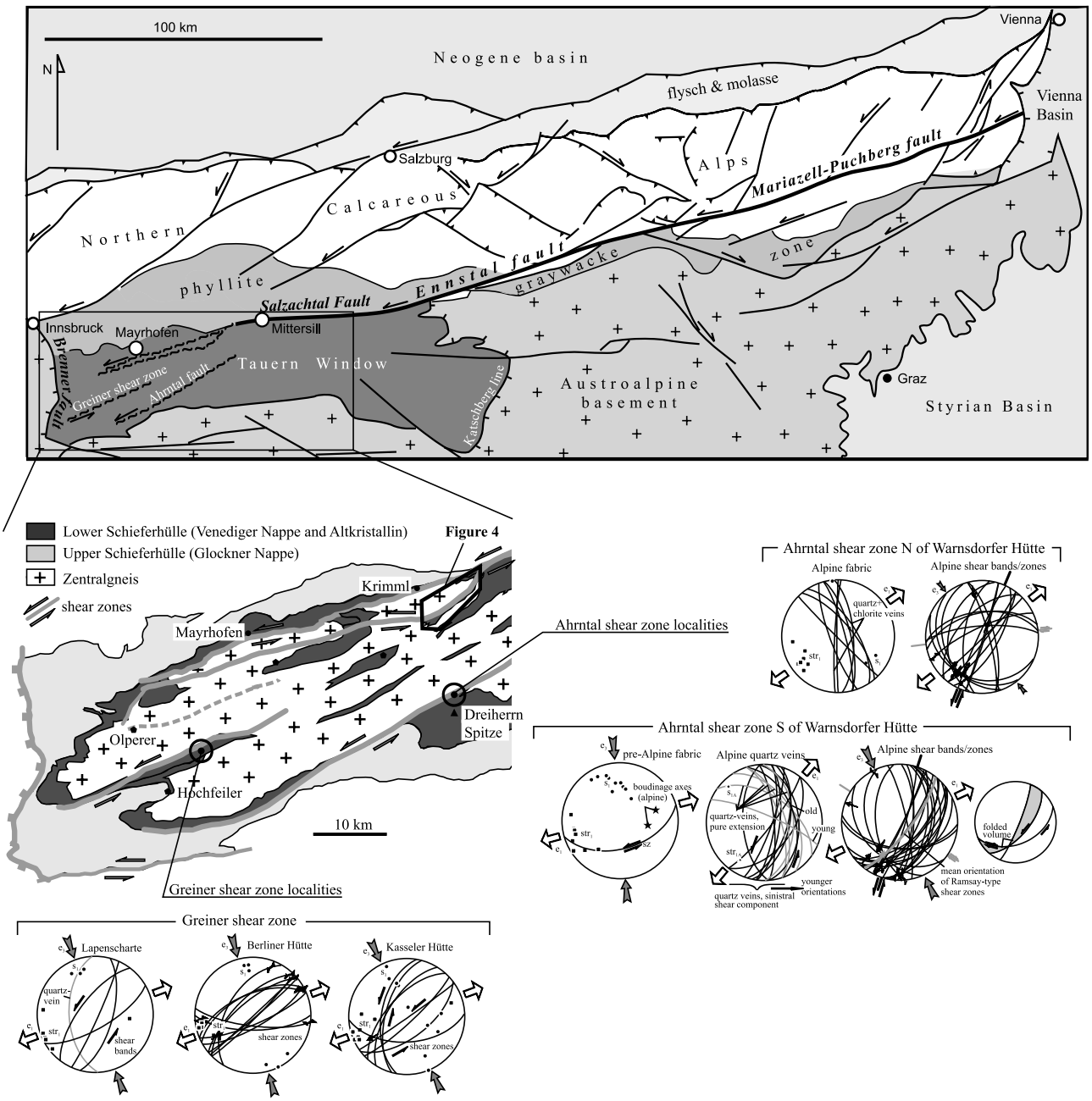

Figure 2. (a) The Salzachtal-Ennstal-Mariazell-Puchberg (SEMP) fault zone [after *Linzer et al.*, 2002] in the framework of the Tertiary tectonic structures of the central and eastern Eastern Alps and the location and structural and kinematic characterization of two (Greiner and Ahrntal) of the three major ductile shear zones of the interior of the central and western Tauern Window. The Rinderkarsee shear zone that connects to the SEMP is southeast of Krimml (geologic contacts after *Bigi et al.* [1990]). Structural data are plotted in lower hemisphere, equal-area stereograms, s_1, first foliation; str_1, first stretching lineations; e_3 to e_1, principal strain directions.

Tauern Window, and along the other large-scale shear zones in the Tauern Window. One strand of the Greiner shear zone (Figure 2) of the western Tauern Window yielded electron microprobe U-Th-Pb monazite ages of 29–20 Ma [*Barnes et al.*, 2004]. Muscovite from a chlorite-muscovite schist from the core of the Ahrntal shear zone and biotite from the central zone of the Rinderkarsee shear zone (Figure 2), the latter studied in this paper (see below), gave latest Oligocene (~24 Ma) $^{40}Ar/^{39}Ar$ cooling ages (Table 1). In contrast, muscovite and biotite from an annealed garnet-hornblende schist from the Greiner shear zone yielded middle Miocene (~15 Ma) $^{40}Ar/^{39}Ar$ ages (Table 1). Along the eastern SEMP, the Vienna basin and relict pull-apart basins demonstrate faulting during the early and middle Miocene [e.g., *Peresson and Decker*, 1997b], leaving the possibility that the eastern portion of the SEMP is younger (15 Ma?) than the western portion (25 Ma?). The absence of a younger, brittle overprint on the ductile shear zones of the

Table 1. New $^{40}Ar/^{39}Ar$ Data[a]

Shear Zone	UTM	Sample	Mineral	J	TFA, Ma	IA (TFA)	Correlation	$^{40}Ar/^{36}Ar$	WMA, Ma	Steps Used	^{39}Ar Used, %
Ahrntal	0292026, 5220107	50801B1	muscovite	0.014376	25.5 ± 1.0	*24.6 ± 0.6*	0.96	415 ± 62	25.0 ± 0.7	5–10/10	93
Greiner	0758146, 5213263	50805B1	muscovite	0.014231	15.4 ± 0.6	*15.4 ± 0.3*	0.99	328 ± 27	15.0 ± 0.4	6–10/10	82
Greiner	0758146, 5213263	50805B1	biotite	0.014231	14.0 ± 0.3	15.3 ± 0.3	0.98	286 ± 22	*14.6 ± 0.3*	2–9/10	66
Rinderkarsee	0288202, 5231406	50729A1	muscovite	0.014231	23.6 ± 0.8	23.5 ± 0.7	0.97	316 ± 32	*23.4 ± 0.8*	2–6, 8–10/10	86

[a]TFA is total fusion age; IA is isochron age; WMA is weighted mean age (preferred age in italics); J is the irradiation parameter; isochron and weighted mean ages are based on fraction of ^{39}Ar listed. Sample descriptions are 50801B1 low-grade phyllitic chlorite-muscovite schist; 50805B1 posttectonically annealed garnet-muscovite-hornblende schist; 50729A1 Zentralgneis granodiorite. Dating specifications are sample weights between 10 and 28 mg; the grain size was $\geq$0.25 mm. Ar/Ar dating is by W. Frank in the CEAL-Laboratory of the Slovak Academy of Sciences, Bratislava, Slovenia.

Tauern Window may be because deformation migrated northward onto the strand of the SEMP that runs along the northern margin of the Tauern Window and the many faults in the northern Calcareous Alps.

2.1. Strike-Slip Deformation at and Beneath the Brittle-Ductile Transition

[10] To investigate deformation along the SEMP at depths where the deformation was changing from brittle-ductile to dominantly ductile, we chose a shear zone in the NE corner of the Tauern Window near Rinderkarsee (a lake), south of Krimml (inset, Figure 2). The steep fabric of the Rinderkarsee shear zone implies that it formed late during the doming of the Tauern Window; otherwise, it would have been rotated to a shallower angle. The Rinderkarsee shear zone is hosted within the relatively homogeneous millimeter- to centimeter-scale granitic Zentralgneis and its much more diverse amphibolite-facies metasedimentary host rocks, the Habach Group (Figures 2–4). In detail, the shear zone consists of a series of three main high-strain zones (a northern shear zone, a central shear zone, and a southern shear zone) separated by low-strain panels. The bulk of the Zentralgneiss in the low-strain panels enjoyed a bulk strain estimated from grain shapes of $\gamma \approx 1$ (Figure 3a).

2.1.1. Northern Shear Zone

[11] Immediately south of Rinderkarsee, a decameter-thick zone within the Zentralgneis contains steeply dipping, NE striking, chiefly meter-scale shear zones. At the grain scale the deformation within the shear zones was brittle-ductile (Figure 3b): ductilely stretched quartz grains have high aspect ratios, whereas feldspars are brittlely deformed.

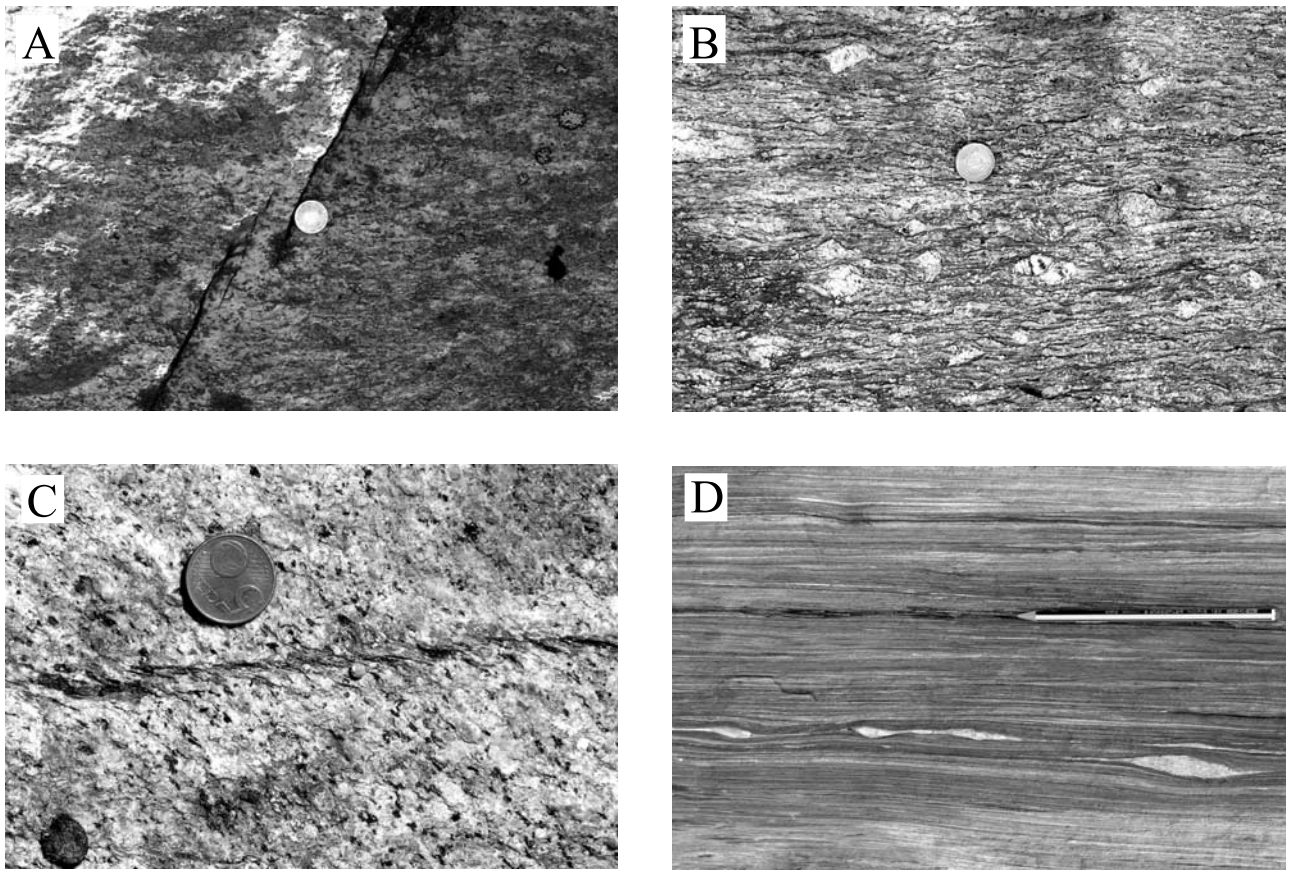

Figure 3. Macroscopic deformation within the Rinderkarsee shear zone. (a) Host Zentralgneis with minimal background ductile strain cut by brittle chlorite-filled tension gash array. (b) Moderate-strain zone in gneiss showing ductile quartz and brittle-ductile feldspar. (c) Brittle-ductile incipient shear zones. (d) Wholly ductile high-strain zone.

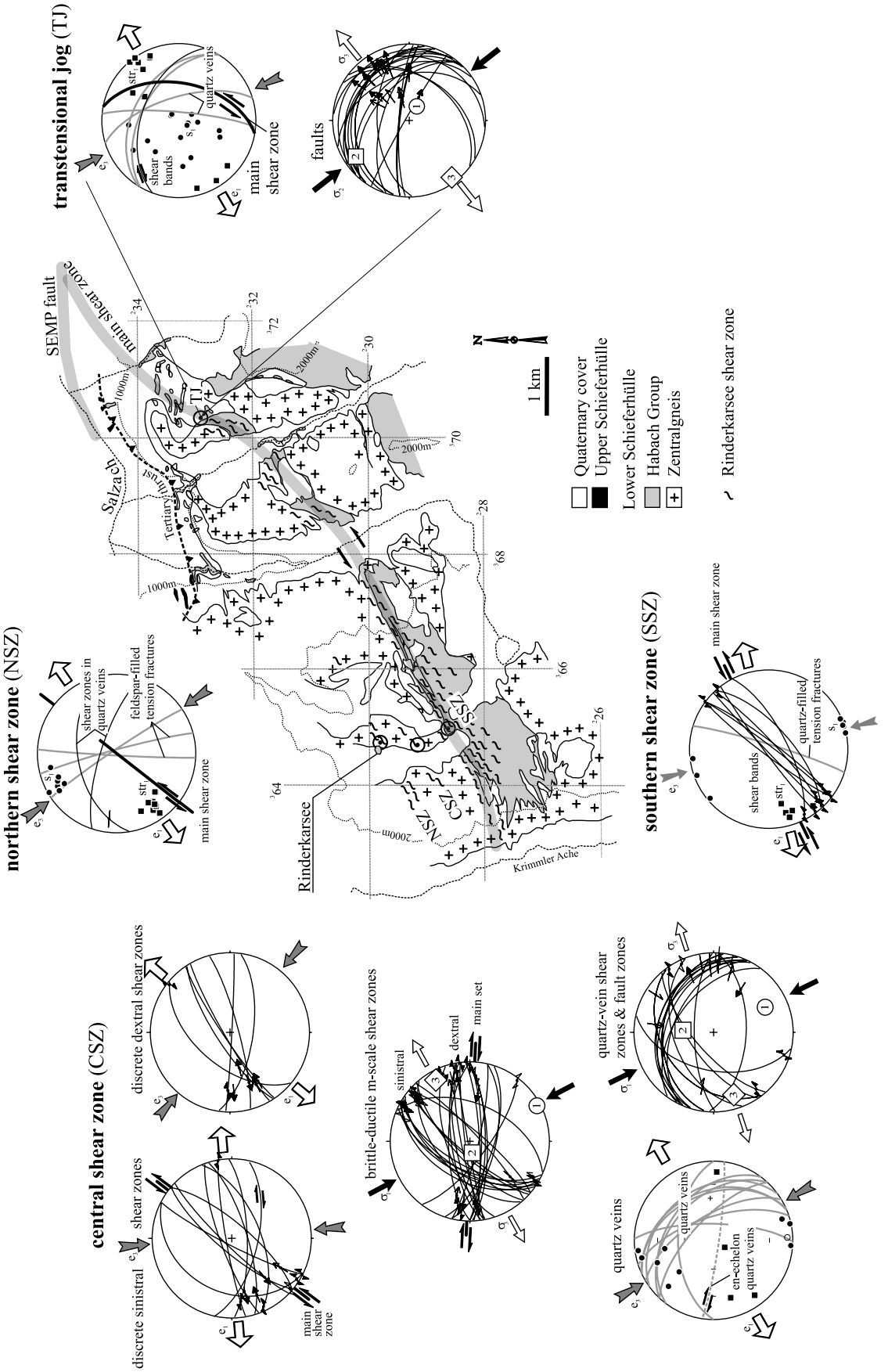
transtensional jog (TJ)
shear bands
quartz veins
main shear zone
faults
SEMP fault
main shear zone
Salzach
Tertiary
1000m
2000m
T1
1 km
N
Quaternary cover
Upper Schieferhülle
Lower Schieferhülle
Habach Group
Zentralgneis
Rinderkarsee shear zone
Rinderkarsee
NSZ
CSZ
SSZ
Krimmler Ache
northern shear zone (NSZ)
shear zones in quartz veins
feldspar-filled tension fractures
main shear zone
southern shear zone (SSZ)
main shear zone
shear bands
quartz-filled tension fractures
central shear zone (CSZ)
discrete dextral shear zones
discrete sinistral shear zones
main shear zone
brittle-ductile m-scale shear zones
sinistral
dextral
main set
quartz-vein shear zones & fault zones
quartz veins
en-echelon quartz veins

Figure 4

The angular difference between the schistosité (S) and cisaillement (C) planes of a weak S-C fabric [*Berthé et al.*, 1979] suggests $\gamma > 2$ [*Ramsay and Huber*, 1983]. Sinistral shear is indicated by an asymmetrically boudinaged aplite dike and the S-C fabric.

2.1.2. Central Shear Zone

[12] The central shear zone is ~450 m farther south (closer to the Habach Group contact) and also hosted in the Zentralgneis. It has a width of ~50 m and consists of at least three generations of structures: the earliest are en echelon arrays of long (decimeter-scale) and narrow (centimeter- to millimeter-scale) subvertical sinistral and dextral shear zones that strike E-NE and are filled with muscovite, biotite, or chlorite. Like the northern shear zone, quartz was ductile and feldspar brittle. These features are truncated by a younger, wider (m scale), and more numerous set of brittle-ductile shear zones that form conjugate sinistral and dextral sets (Figure 3c); a few are brittle and bear chlorite. The youngest structures are sheared quartz veins, tension-gash arrays, and minor brittle faults (Figure 3a).

2.1.3. Southern Shear Zone

[13] Shear zone width and strain magnitude indicate that the southern shear zone is the main strand of the Rinderkarsee shear zone at our study site. It is separated from the central shear zone by a low-strain panel ~600 m wide. It straddles the Zentralgneis-Habach Group contact: the Zentralgneis is phyllonitic over a 3-m-wide zone, whereas the less competent rocks of the Habach Group are mylonitic over a zone $\geq$100 m wide (Figure 3d). Like the northern shear zone, it consists of sinistral NE striking subvertical meter-scale shear zones. Strain, estimated from the relative amount of grain size reduction, is greatest in this southern shear zone, likely because of the competence contrast across the contact. At the outcrop scale, the rock has the typical "ductile" appearance of a mylonite: fabrics are homogeneous at the meter and smaller scale, except for localized slip along boudin surfaces.

2.1.4. Shear Zone Kinematics

[14] We used fault striae analysis to analyze the kinematics of the Rinderkarsee shear zones. The sense of motion on faults and shear zones was determined using Riedel shears, S-C fabrics, drag of foliation, and fibrous mineral growth [e.g., *Petit*, 1987]. A confidence level, based on the type, abundance, and clarity of the indicator, was assigned to each sense of motion determination, and used as a weighting factor in our kinematic analysis. We used the computer program package of *Sperner et al.* [1993] for fault slip analysis to calculate the orientation of the principal stress axes [*Angelier*, 1984]. Our brittle-ductile fault data are best interpreted by using a fracture angle of 45° rather than 30°; this higher angle is in agreement with experimental data that links higher fracture angle with higher confining pressures [*Mogi*, 1974].

[15] The simple NE striking sinistral shear zones in the northern and southern shear zones accommodated ~NNW and ~ENE trending shortening and extension, respectively (Figure 4), accommodating orogen-parallel extension and orogen-perpendicular contraction along with eastward extrusion of Tauern Window. The central shear zone is more complicated. The orientations of the early sinistral and dextral en echelon shear zones shear zones, the significant overlap in their orientations, and their millimeter- to centimeter-scale offsets, suggest that rather than being simple conjugate pairs, these early shear zones may be related to lithologic heterogeneities in the Zentralgneis. While these shear zones share an extension direction with earlier structures, both the principal extension direction, e_1, and the intermediate strain axis, e_2, vary by as much as 30°. This variation may be related to the interaction of a vertical shortening component with the dominant NNW-ESE shortening. However, the main brittle-ductile faults of the central shear zone accommodated ~NW directed shortening and ~NE directed extension, similar to the northern and southern shear zones. The youngest structures (sheared quartz veins, tension gash arrays, and minor brittle faults) are kinematically compatible with this.

[16] Although overprinting relationships within each of the northern, central, and southern shear zones constrain the relative timing of structures within each of those zones, we cannot constrain whether these three shear zones were active together or in sequence. If the general change from brittle-ductile deformation to brittle deformation observed in the central and southern shear zones is indicative of the history of the entire Rinderkarsee shear zone, we infer that the earliest deformation was the ductile amphibolite-facies (see below) deformation typified by the southern shear zone, midstage deformation was brittle-ductile typified by the bulk of the structures in the central and northern shear zones, and the youngest deformation was brittle and typified by the minor cracks/veins of the central shear zone.

2.2. Optical Microstructures

[17] To evaluate the grain-scale deformation mechanisms within the Rinderkarsee shear zone, we studied three primary microstructural types: (1) an early(?) high-strain ductile mylonite from the southern shear zone, (2) a moderate-strain brittle-ductile shear zone from the central shear zone, and (3) the late stage(?) tip of a millimeter-scale brittle-ductile shear zone from the central shear zone. The undeformed host gneiss is a biotite-bearing granite with

Figure 4. Simplified geological map (modified from *Kupferschmied* [1994]) and structural data of the Rinderkarsee shear zone and its likely connection with the SEMP along the Salzach valley. Samples for this study were collected along a traverse that runs south from the Rinderkarsee. Equal-area, lower hemisphere projections, and strain orientations (e_3, e_1) were estimated from the average orientation of foliation and stretching lineation; principal stress orientations (σ_1, σ_3) were calculated with a fracture angle of 45°. Southern and main shear zone (SSZ), foliation (s_1, filled circles), lineation (str_1, filled squares), shear bands with flow direction (arrows), tension fractures, and quartz-filled tension fractures are indicated. Central shear zone (CSZ) with quartz veins, lineations, and foliations, brittle-ductile conjugate shear zones, discrete sinistral and dextral shear zones and late quartz-filled shear zones is shown. Northern shear zone (NSZ) with lineation, foliation, quartz vein shear zones, and feldspar-filled tension fractures is shown. The Rinderkarsee shear zone forms as transtensional jog, exemplified by rotated foliation orientations, quartz veins, and normal faults, before it connects to the SEMP.

~1 mm grains of 5% biotite, 35–55% quartz, 25–40% alkali feldspar, and 10–25% plagioclase. Plagioclase includes ~5 vol % of ~10 μm diameter muscovite + quartz grains, presumably formed from decomposition of the K_2O component in the plagioclase (see below). All the alkali feldspar is "interlocking" antiperthite [e.g., *Alling*, 1938] (average bulk grain composition of $an_{00}ab_{52}or_{48}$; measured by electron probe) composed of 10–100 μm wide intergrowths of $an_{00}ab_{99}or_{01}$ (albite) and $an_{00}ab_{05}or_{95}$ (microcline) and is referred to as "K-feldspar."

2.2.1. High-Strain Ductile Mylonite

[18] The highest-temperature and highest-strain rocks are the mylonitic rocks of the Habach Group from the southern shear zone (Figure 5a). Mylonitic amphibolites are composed chiefly of prismatic 50-μm-long hornblende with minor undulatory extinction and equant 20 μm plagioclase. Mylonitic quartzofeldspathic rocks consist predominantly of subequal amounts of plagioclase, quartz, and biotite. Rare plagioclase porphyroclasts up to 1 mm in diameter have patchy undulatory extinction, subgrains, deformation twins, and core-and-mantle recrystallization microstructures; the bulk of the plagioclase are 20–50 μm, have axial ratios of ~2:1, sweeping undulatory extinction, and straight to curved grain boundaries. Where not pinned by other phases, quartz reaches 200 μm and has sweeping undulatory extinction, well-defined subgrains, and dentate grain boundaries; most of the quartz grains are pinned to <50 μm.

2.2.2. Moderate-Strain Brittle-Ductile Shear Zone

[19] Deformation within the moderate-strain central shear zone was accommodated by mixed brittle and ductile deformation (Figure 5b). Millimeter-scale quartz grains in the host gneiss have been deformed into polycrystalline clots of ~200-μm-scale grains with embayed boundaries, pervasive undulatory extinction, island grains, and numer-

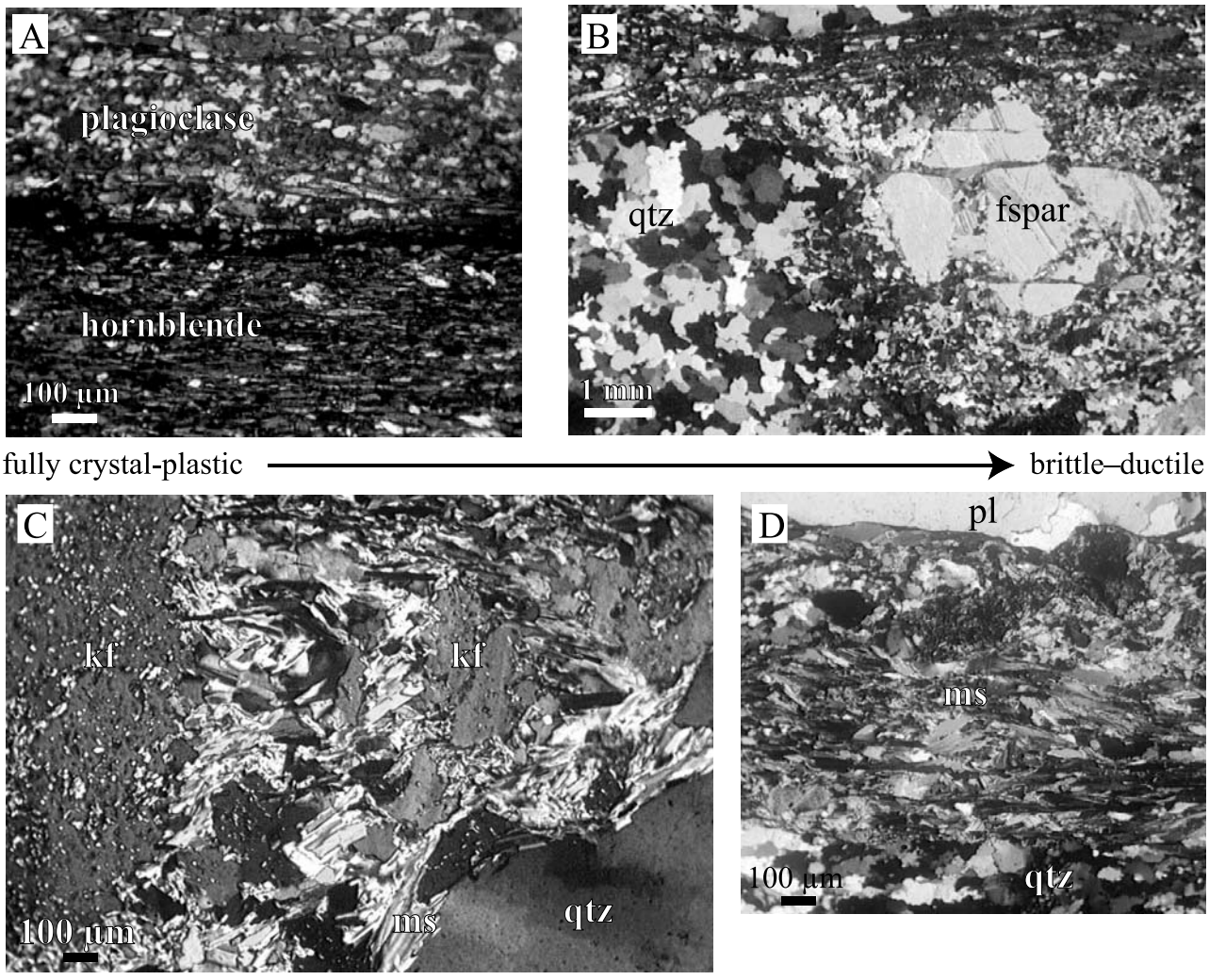

Figure 5. Rinderkarsee shear zone microstructures. (a) Mylonitic amphibolite from southern shear zone showing crystal-plastic deformation of amphibole and feldspar (sample 5729G1). (b) Brittle-ductile fabric in southern shear zone Zentralgneis with brittle feldspar and ductilely deformed quartz. Feldspar fractures are filled with recrystallized quartz, muscovite, and calcite (5729F1). (c) Alteration of K-feldspar to muscovite (5729H1B). (d) A more mature, millimeter-scale shear zone formed via the linkage of muscovite-rich grain boundaries. Cracking and fluid infiltration produced the reaction K-feldspar + fluid → muscovite + albite. This muscovite-producing reaction served to drive both strain localization and dynamic recrystallization in K-feldspar via transformational plasticity.

ous subgrains, all features typical of regime 3 of *Hirth and Tullis* [1992]. K-feldspar and plagioclase porphyroclasts have brittle fractures filled with epidote, muscovite, and quartz, deformation lamellae, deformation twins, patchy undulatory extinction, and local core-and-mantle microstructures. Strain is concentrated in quartz- and mica-rich zones that anastomoze around brittlely deformed K-feldspar and plagioclase porphyroclasts.

2.2.3. Brittle-Ductile Shear Zone Tip

[20] The millimeter-scale tips of several of the late, long, narrow shear zones of the central shear zone show unexpected features. The rock hosting the shear zones shows only brittle-ductile deformation: quartz shows microstructures typical of grain boundary migration (i.e., regime 3 of *Hirth and Tullis* [1992]), and feldspars have brittle fractures, mechanical twins, deformation lamellae, undulatory extinction and some subgrains (Figure 5c). The feldspar cataclasis was accompanied by the growth of muscovite. This breakdown localized deformation in muscovite-rich grain boundaries, which eventually connected to form throughgoing, discrete shear zones (Figure 5d). Within these discrete shear zones, all grains (K-feldspar, plagioclase, and quartz) are pervasively recrystallized.

2.3. Electron Backscatter Diffraction Microanalysis

[21] Critical additional information regarding the grain-scale deformation was obtained from electron backscatter diffraction (EBSD; see Appendix A). We used two spatial scales of EBSD to characterize the microstructural evolution of the Rinderkarsee shear zone: (1) sample-scale determinations of lattice preferred orientations (LPO; same as crystallographic preferred orientation) and (2) finer-scale maps of selected smaller areas to determine LPOs, grain shapes, grain sizes, intragrain lattice rotation, and intergrain orientation relationships.

2.3.1. High-Strain Ductile Mylonite

[22] The microstructure of a typical mylonitic sample from the southern shear zone is exhibited in Figure 6; this sample (50729G6) is a metaconglomerate from the Habach Group a few meters from the contact with the Zentralgneis. The sample grain size is fairly uniform although the plagioclase are the finest (Figure 6a); the feldspar and quartz grains are all isolated, but both, particularly quartz, which is more abundant and coarser, show subgrains. Plagioclase, K-feldspar, and quartz all have aspect ratios of ~2:1, determined by processing of EBSD data. Rare plagioclase porphyroclasts have maximum dimensions of 500–700 μm and well-developed strain shadows filled with recrystallized quartz (Figure 6b). These plagioclase porphyroclasts show 5°–8° of misorientation from core to rim (Figure 6c), and the more abundant 50–100 μm matrix plagioclase grain show 3°–6° misorientation from core to rim. The matrix feldspar grains have weak LPOs (multiples of uniform distribution (MUD) $\leq$ 2), with [001] subparallel to the X strain axis and poles to (010) subparallel to the Z strain axis (Figure 6e). All the quartz grains, regardless of whether they are matrix grains or hosted in plagioclase strain shadows, show a random distribution of grain orientations (MUD < 2) (Figure 6c). Individual quartz grains within strain shadows have <5° of misorientation from core to rim that are compatible with rotation around the *c* axis. Quartz matrix grains yield misorientation angle distributions for neighbor pairs and random pairs that are equivalent at the 80% confidence level (using the Kolmogorov-Smirnov test, d = 1.08) [*Wheeler et al.*, 2001] (Figure 6f). Recrystallized quartz grains in the strain shadow of a plagioclase porphyroclasts show a greater correlation between neighbor and random pairs (d = 0.75; confidence interval <80%), and have a peak of misorientations between 2° and 10° (Figure 6g).

[23] To assess whether these weak LPOs are typical of the mylonite zone, two other high-strain rocks of different composition were also measured. Sample 50729G4 is a biotite-rich gneiss from the Habach Group and 50729G5 is an aplitic Zentralgneis dike intruding the Habach Group. Both have weak LPOs (Figures 7a and 7b) similar to mylonitic sample 50729G6.

2.3.2. Moderate-Strain Brittle-Ductile Shear Zone

[24] Moderate-strain brittle-ductile shear zones (e.g., sample 50729F3) contain quartz augen up to 2 mm, recrystallized quartz grains, and mica-rich foliation planes. Individual quartz augen larger than ~50 μm show a strong ''single-crystal'' fabric with their *c* axes subparallel to the Z strain axis (Figure 8b) and outward increasing misorientations of up to 5° between core and rim that show rotation about poles to prism planes. Matrix quartz grains show a weaker, but still significant LPO with *c* axes subparallel to Y and dispersed ⟨a⟩ axes (Figure 8c). The presence of distinct fabrics in the quartz augen and matrix quartz suggests that the quartz augen are relicts of an older fabric and are unfavorably oriented for slip. In contrast to the quartz grains, the feldspar porphyroclasts contain no optically visible subgrains and are transected by fractures filled with neoblastic quartz and muscovite.

2.3.3. Brittle-Ductile Shear Zone Tip

[25] Late, millimeter-scale brittle-ductile shear zone tips are typified by Zentralgneis sample 50729H1b (Figure 9). The feldspar grains have a strong LPO (Figures 9d and 9e) characterized by [010] subparallel to the X strain axis and poles to (001) subparallel to the Z strain axis. Quartz grains have a modest LPO (MUD $\leq$ 6) with *c* subparallel to Z and distributed ⟨a⟩ axes (Figure 9e). Individual grains of feldspar and quartz have aspect ratios of ~2:1 and show core-rim misorientations of 4°–8° (Figure 9f); the intragrain lattice rotations in quartz are compatible with rotation about the *c* axis. Quartz neighbor pairs show an abundance of low misorientation angles compared to random pairs of grains, suggesting subgrain rotation recrystallization (Figure 9g).

3. Discussion

3.1. Quartz Deformation Mechanisms at Rinderkarsee

[26] By what grain-scale mechanisms did the quartz grains in the Rinderkarsee shear zone deform? Clear evidence of crystal plasticity mandates some combination dislocation glide or creep, solution transfer creep, and grain boundary sliding.

[27] A group of microstructural observations argue in favor of dislocation creep: (1) All the Rinderkarsee shear zone samples show optical quartz microstructures indicative of high grain boundary mobility and regime 3 dynamic recrystallization [e.g., *Hirth and Tullis*, 1992; *Stipp et al.*, 2002]. (2) The medium-strain shear zone (Figure 8) and the shear zone tip (Figure 9) have strong quartz LPOs. (3)

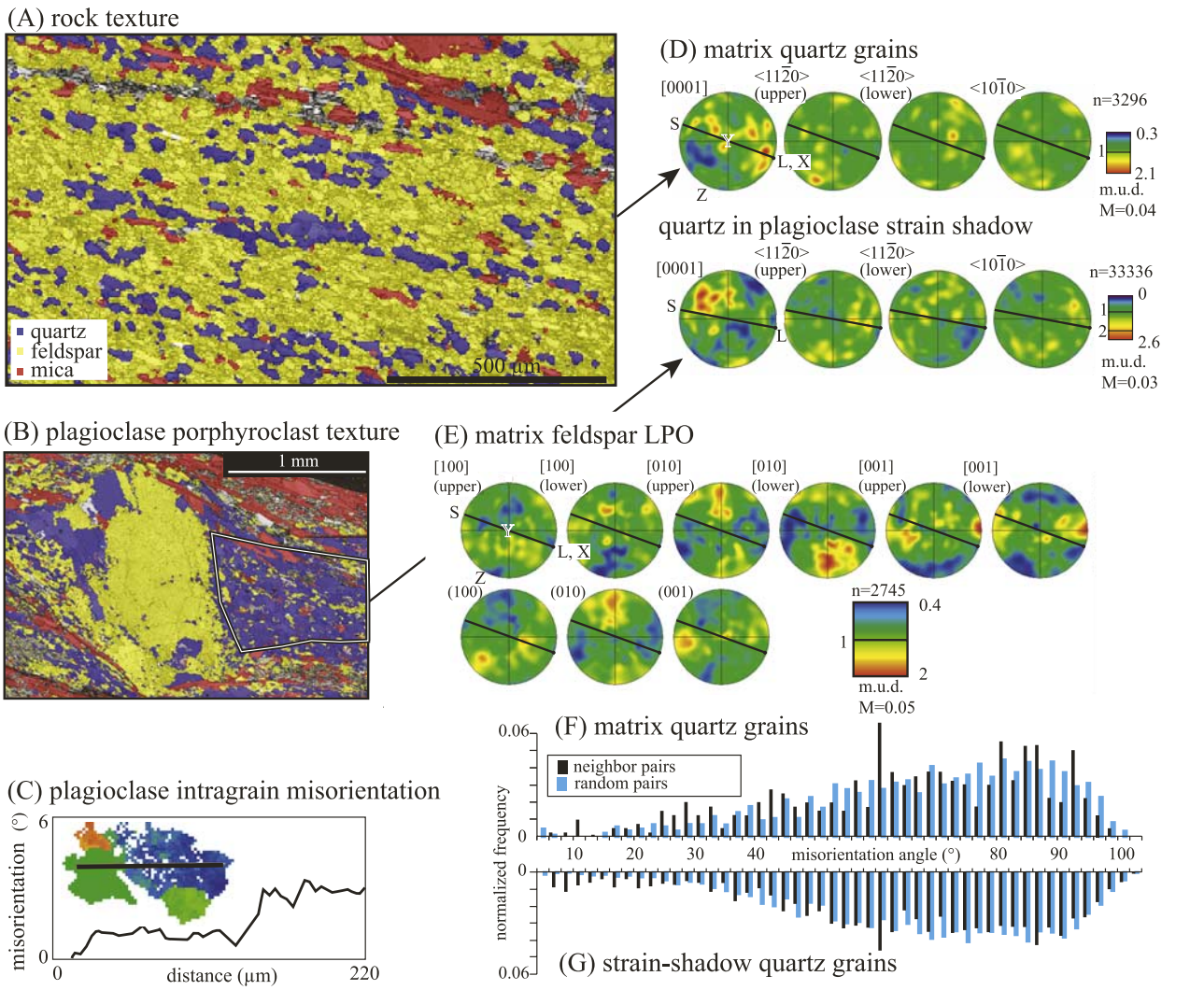

Figure 6. Textures and LPOs of mylonitic sample 50729G6, a Habach Group metaconglomerate. (a) Texture map; a strong shape preferred orientation in all grains. (b) Plagioclase porphyroclast texture. (c) Misorientation of 3° between core and rim of a plagioclase grain, indicating that subgrain rotation was an active recovery mechanism. (dD) LPO for quartz grains within the feldspar strain shadow; implying some basal-⟨a⟩ glide. (e) Plagioclase LPO; weak, with [001] subparallel to the X strain axis and poles to (010) subparallel to the Z strain axis. (f) Misorientation-angle distributions for neighbor pairs and random pairs of quartz matrix grains; equivalent at the 80% confidence level (using the Kolmogorov-Smirnov test, d = 1.08). (g) Misorientation angle distributions for neighbor pairs and random pairs of recrystallized quartz grains in the strain shadow of a plagioclase porphyroclast; stronger correlation between neighbor and random pairs (d = 0.75; confidence interval <80%). The 60° peak is a result of Dauphiné twinning.

Individual quartz grains show clear intragrain lattice rotation. (4) The statistically significant difference between the distribution of misorientation angles between neighbor pairs and random pairs of quartz grains in the plagioclase strain shadow of mylonitic sample 50729G6 and in the shear zone tip sample 50729H1b implies that these neighboring quartz grains are related through subgrain rotation recrystallization [*Lloyd et al.*, 1997; *Wheeler et al.*, 2001].

[28] In contrast to the above observations that speak in favor of dislocation glide or creep, other microstructural observations indicate the activity of other deformation mechanisms: (1) The similarity in the misorientation distributions of the neighbor pairs and random pairs in the matrix quartz of mylonitic sample 50729G6 implies that those grains are not related through dislocation creep and (2) the quartz LPOs in the mylonite samples are weak to random (Figures 6 and 7).

[29] These microstructural observations, combined with the fine grain size and equant shapes of the quartz grains, render it most plausible that the dominant quartz deformation mechanism in the samples with weak LPOs was dislocation creep-accommodated grain boundary sliding [*Boullier and Gueguen*, 1975; *Rutter et al.*, 1994]. Cathodoluminescence microscopy was used to look in the moderate-strain, mylonitic and shear zone tip samples for evidence of cracking, dissolution, or precipitation of quartz that might be correlated with the fluid required for muscovite formation from feldspar; none was observed.

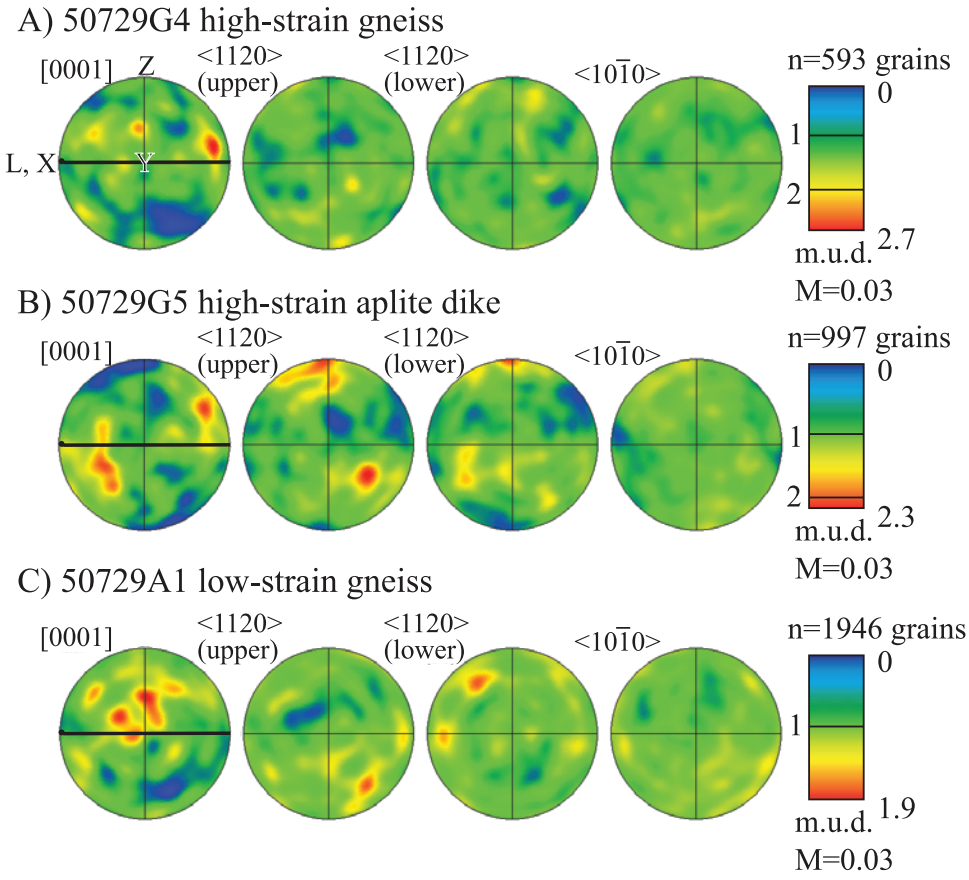

Figure 7. Weak to random quartz LPOs. (a, b) High-strain rocks from southern shear zone. (c) low-strain rock hosting shear zone in Figure 9.

3.2. Plagioclase Deformation Mechanisms at Rinderkarsee

[30] Plagioclase in mylonitic samples show optical microstructures and intragrain lattice orientation indicative of dislocation creep. The absence of microcracks and the fine equant grain size are compatible with dislocation creep-accommodated grain boundary sliding in feldspar in the high-strain mylonite; this is in spite of the fact that feldspar does not form isolated, pinned grains in the mylonitic rocks.

[31] Plagioclase in shear zone tips show optical microstructures and intragrain lattice orientation (e.g., Figure 9) indicative of dislocation creep. These features, combined with the thin section scale microcracks discussed above, imply that feldspar deformation in the shear zone tips involved a combination of microcracking, dislocation creep, and grain boundary sliding. Outside the millimeter-scale shear zones, there is a weak to random LPO in all phases. Within these shear zones, however, all phases have strong LPOs. There are also significant misorientations across grains of all phases, and a statistically significant difference between neighbor pair and random pair misorientations. This reveals that the active recrystallization mechanisms within nascent shear zones included subgrain rotation and grain boundary migration.

3.3. Dislocation Glide Systems at Rinderkarsee

[32] Our data provide two means of determining which slip systems were active during the formation of the Rinderkarsee shear zone: multigrain LPOs and intragrain rotations. In the mylonitic rocks (Figures 6 and 7), the feldspar and quartz LPOs are weak, but quartz intragrain rotation in 50729G6 suggests basal slip in the ⟨a⟩ direction. In the moderate-strain, brittle-ductile central shear zone (Figure 8), the LPOs and intragrain lattice rotations suggest prism ⟨a⟩ slip in quartz matrix grains and basal ⟨a⟩ slip in quartz porphyroclasts. Feldspars in the same shear zone yielded no LPOs, have no subgrains, and are transected by fractures, indicating brittle deformation. The LPOs and intragrain rotations from the shear zone tips (Figure 9) indicate a combination of basal and prism ⟨a⟩ slip in quartz and [010](001) slip in feldspar.

3.4. Summary of Deformation Mechanisms at Rinderkarsee

[33] In summary, the shear zone tips are interpreted to have formed by dislocation creep in quartz and microcracking, dislocation creep, and grain boundary sliding of feldspar. The moderate-strain samples deformed via quartz dislocation creep and plagioclase cataclasis in quartz-rich samples and dislocation creep-accommodated grain boundary sliding of quartz and cataclasis + dislocation creep of plagioclase in quartzofeldspathic samples. The high-strain samples formed through dislocation creep-accommodated grain boundary sliding of quartz and feldspar.

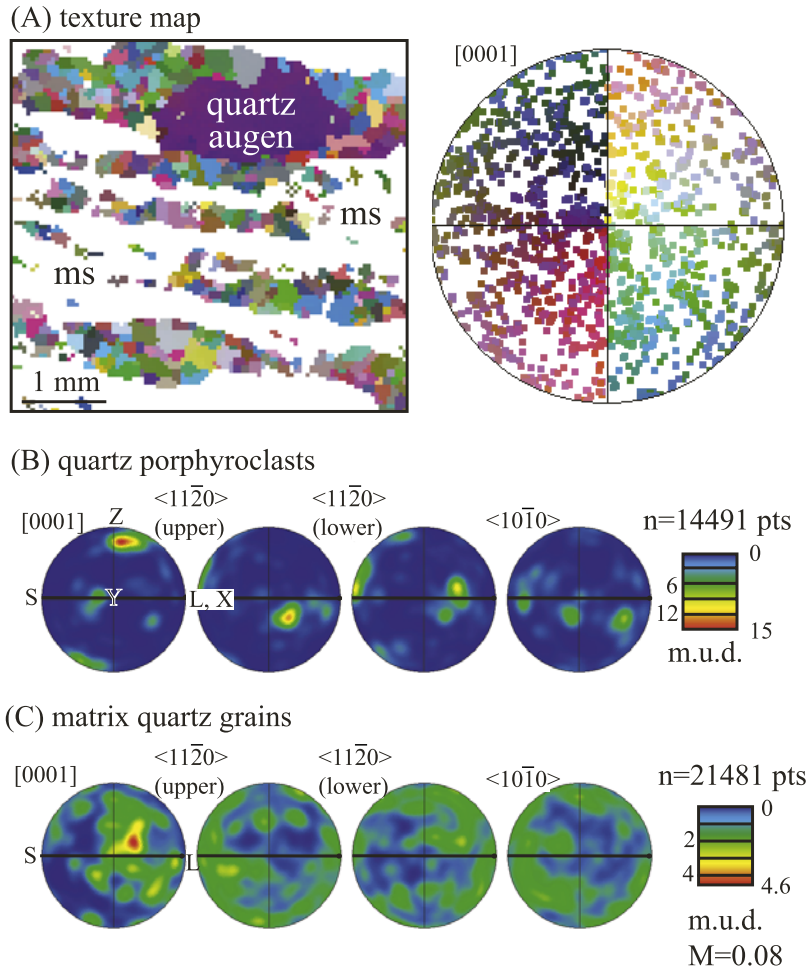

Figure 8. Microstructure and quartz LPO of moderate-strain brittle-ductile quartz-muscovite schist 50729F3. In the equal-area, lower hemisphere stereonets, heavy line shows trace of foliation, S; dot shows lineation, L. (a) Microstructure map, with quartz grains colored by *c* axis orientations shown in stereonet (ms, muscovite). (b) LPO of quartz porphyroclasts, dominated by grains with *c* axes parallel to the Z strain axis. (c) LPO of matrix quartz grains, suggesting prism ⟨a⟩ slip.

3.5. Transformational Plasticity at Rinderkarsee

[34] The microstructures described above indicate that the late, small-scale shear zones at Rinderkarsee formed where fluid influx converted K-feldspar into muscovite. The neoblastic muscovites then served to localize deformation, forming throughgoing, discrete shear zones. K-feldspar, plagioclase, and quartz in these zones show optical and EBSD evidence of dynamic recrystallization even though the feldspars outside the shear zones remained brittle.

3.6. Regional Extent of Rinderkarsee Shear Zone

[35] *Rosenberg et al.* [2007] mapped the Rinderkarsee shear zone 80 km farther west from our study area as part of their Ahorn shear zone (Figures 2 and 10). They report a westward reduction in strain partitioning: the one to hundreds of meter-wide shear zones separated by ~500 m low-strain panels observed at Rinderkarsee gradually give way to a more distributed ductile shear zone as much as 2 km wide. They also document a temporal transition from early amphibolite-facies deformation at ≥500°C in which quartz and plagioclase were ductile, to late greenschist-facies deformation at ≤300°C in which quartz was undergoing dislocation glide, but not creep.

3.7. Deformation Depth at Rinderkarsee

[36] Constraining the depth of deformation at Rinderkarsee is not straightforward because of an absence of rock types suitable for barometry, but can be estimated crudely. If the deformation conditions of the Greiner shear zone, 6–8 kbar and 500–570°C [*Selverstone et al.*, 1984], represent a thermal steady state apropos to the entire Tauern Window, the deformation temperature range of 500–300°C inferred for the Rinderkarsee area corresponds to a depth range of ~24–14 km (assuming a density of 2.75 g/cm^3). If our biotite ^{40}Ar/^{39}Ar age from the Rinderkarsee shear zone of ~24 Ma represents cooling through the standard closure temperature of ~350–300°C [*Dunlap*, 2000], this was at a depth of ~16–17 km. This agrees with the overall exhumation history of the Tauern Window noted earlier: ~25 km depth at 30 Ma, ~10–15 km at 25–17 Ma, and ~4 km by 7 Ma [*Oxburgh et al.*, 1966; *Cliff et al.*, 1985; *Spear and Franz*, 1986; *von Blanckenburg et al.*, 1989; *Christensen et al.*, 1994].

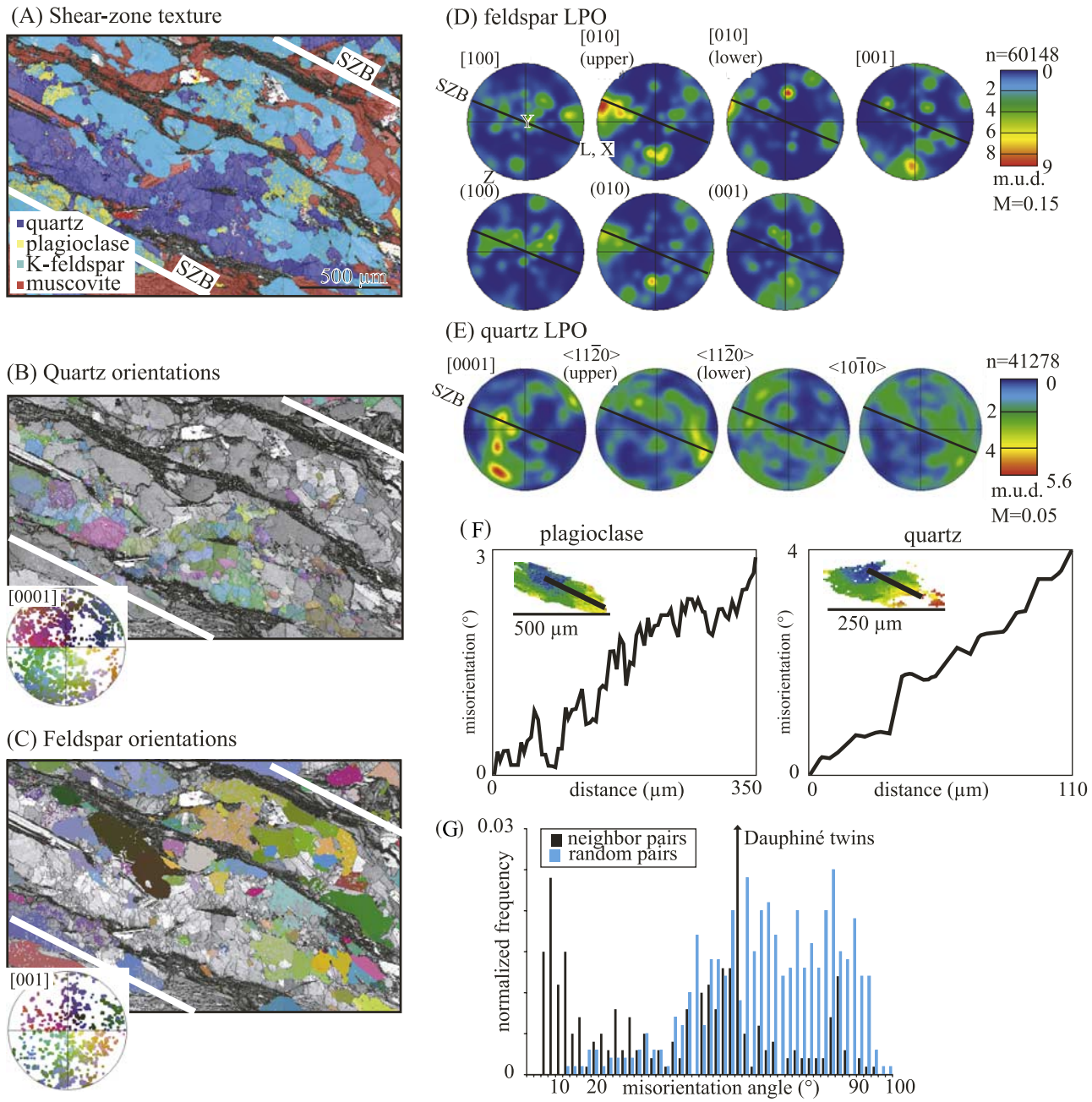

Figure 9. Shear zone sample 50729H1b from the Zentralgneis. In contrast to minerals outside shear zones, dislocation creep was important within shear zones. (a) Shear zone texture; SZB, shear zone boundary. (b) Texture map, with quartz grains colored by *c* axis orientations shown in stereonet. (c) Texture map, with feldspar grains colored by *c* axis orientations shown in stereonet. (d, e) Strong feldspar and quartz LPOs (maximum MUD of 5–15), implying that deformation in the shear zones occurred via a combination of basal ⟨a⟩ and prism ⟨a⟩ slip in quartz and [010](001) slip in feldspar. (f) Lattice misorientations within individual grains. The 3°–4° gradual change suggests dynamic recrystallization via subgrain rotation. (g) Significantly different misorientation angle distributions for quartz shear zone grains for neighbor pairs and random pairs. High frequency of quartz neighbor pairs with small misorientation angles points to subgrain rotation recrystallization.

3.8. Implications for the Brittle-Ductile Transition in Continental Crust

[37] Let us now return to the three questions posed in the introduction about the general applicability of the brittle-ductile transition model in Figure 1.

[38] 1. The Rinderkarsee shear zone is not a single strand but is composed of 1- to 100-m-wide high-strain shear zones separated by ~500-m-wide low-strain panels; macroscopic deformation in the shear zones varied from ductile to brittle-ductile to brittle. The bulk of the strain was

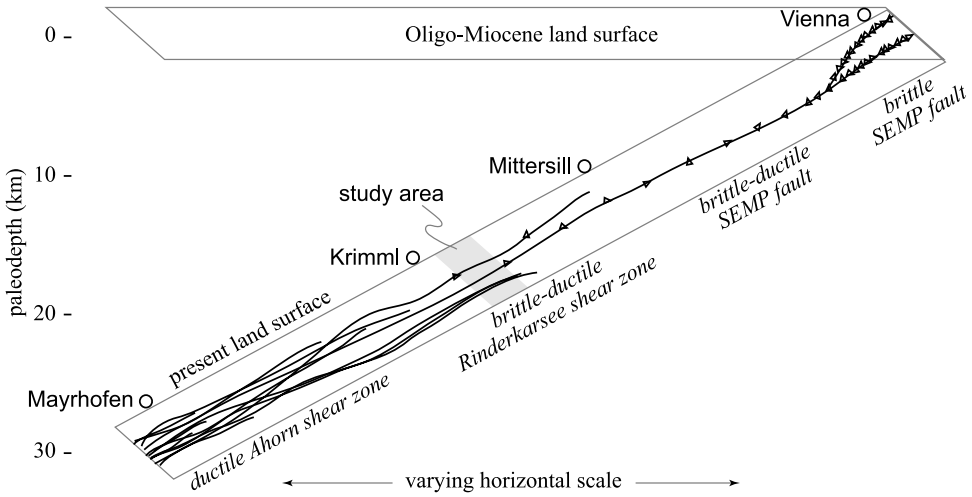

Figure 10. Reconstruction of the active strike-slip SEMP fault system highlighting the change in deformation style from a discrete brittle fault zone at shallow levels [*Linzer et al.*, 2002] to a series of brittle-ductile and ductile shear zones at 15–25 km depth (this study) to a 2-km-wide ductile shear zone [*Rosenberg et al.*, 2007]. The reconstruction is necessarily schematic and greatly simplified, with major uncertainties in paleodepth and ages of various structures. Triangles indicate brittle deformation.

accommodated by the southernmost, ~100 m thick ductile shear zone.

[39] 2. A broad range of deformation mechanisms were active, depending on the type of crystal, the type of rock, and the style of the shear zone. All grains in the largest, ductile shear zone deformed via dislocation creep-accommodated grain boundary sliding. The moderate-strain shear zones are similar, but feldspar deformed principally by microcracking. The thinnest, incipient shear zones developed in muscovite-rich zones formed from hydration of feldspar; all phases within deformed by dislocation creep. Addressing this variation would improve computational models of the brittle-ductile transition.

[40] 3. The alteration of feldspars to phyllosilicates is a recognized form of transformational plasticity in fault zones that has two principal effects: the growth of weak phyllosilicates weakens the entire rock, promoting deformation of feldspar and quartz, and the reduction in grain size can promote diffusion-accommodated grain boundary sliding or solution transfer creep [*Evans*, 1988; *Janecke and Evans*, 1988; *Wintsch et al.*, 1995; *Hippertt*, 1998; *Imber et al.*, 2001; *Ingles et al.*, 1999; *Gueydan et al.*, 2003]. What is novel about the Rinderkarsee shear zone is that the growth of weak phyllosilicates promoted the formation of shear zones in which the dominant deformation mechanism was dislocation creep.

4. Conclusions

[41] The Rinderkarsee shear zone provides an excellent opportunity to study fault structure at the transition from brittle-ductile to ductile deformation. It is overall a brittle-ductile shear zone, but is composed of narrow, highly localized (1–100 m wide) zones of concentrated strain that are either brittle-ductile or ductile.

[42] The highest-strain zone is also the widest (100 m), and represents a discrete, downward continuation of the Salzach fault into the ductile midcrust. This zone is mylonitic, but shows weak lattice-preferred orientations, implying that the bulk grain-scale deformation of quartz and feldspar was dislocation-assisted grain boundary sliding. Moderate-strain brittle-ductile shear zones formed via quartz dislocation creep and plagioclase cataclasis in quartz-rich samples and via dislocation creep-accommodated grain boundary sliding of quartz and cataclasis + dislocation creep of plagioclase in quartzofeldspathic samples. Millimeter-scale incipient shear zones show strong lattice-preferred orientations and dynamic recrystallization of all phases, including plagioclase and K-feldspar, even though feldspars outside the shear zones were undergoing cataclasis. This unusual feldspar plasticity was accompanied by fluid-driven alteration of K-feldspar to muscovite that served to localize strain along muscovite-rich grain boundaries that developed into throughgoing grain-scale shear zones.

Appendix A: EBSD Methods

[43] Thin sections were polished for 1 h with 1 μm and 0.25 μm diamond polishing compound, for 12–14 h in colloidal silica, and then carbon coated. They were analyzed in a JEOL 6300 scanning electron microscope fitted with an HKL Nordlys EBSD camera. They were inclined 70° to the incident beam. Working conditions were: 20 kV acceleration voltage, ~4.5 nA beam current, <1 μm spot size, and 25 mm working distance. Diffraction patterns were collected and indexed using CHANNEL 5 HKL software. By carefully examining the effect of parameters such as Hough transform, number of reflectors, minimum and maximum number of bands detected, and the chosen match unit, we are confident that the CHANNEL software indexed the correct phase >95% of the time. Samples were analyzed in both coarse and fine mode. Coarse scans used a step size of 50 μm designed to gather the bulk LPO of the sample and covered an area of 1 cm^2, whereas fine scans used a step size of 4 μm to examine textural attributes of samples and individual grains. We used the noise reduction system within the HKL software, carefully

comparing our maps to the band contrast and fore scatter images to fill grains without artificially growing them.

[44] **Acknowledgments.** Funded by NSF grants EAR-0309995 and EAR-0309542 and DFG grant Ra 442/19. Kurt Decker (Universität Wien), Bernd Lammerer (LMU München), and Franz Neubauer (Universität Salzburg) graciously shared their SEMP expertise. Nicholas Barth was mountain goat 2. We thank Charles Sammis for helpful discussions and Claudio Rosenberg for a preprint of his Tauern shear zone paper. Joe White and Wolfgang Frisch provided helpful reviews.

References

Alling, H. L. (1938), Plutonic perthites, *J. Geology*, *46*(2), 142–165.
Angelier, J. (1984), Tectonic analysis of fault slip data sets, *J. Geophys. Res.*, *89*, 5835–5848.
Barnes, J. D., J. Selverstone, and Z. D. Sharp (2004), Interactions between serpentinite devolatilization, metasomatism and strike-slip strain localization during deep-crustal shearing in the Eastern Alps, *J. Metamorph. Geol.*, *22*, 283–300.
Behrmann, J. H., and W. Frisch (1990), Sinistral ductile shearing associated with metamorphic decompression in the Tauern Window, eastern Alps, *Jahr. Geol. Bundesanst.*, *133*, 135–146.
Berthé, D., P. Choukroune, and D. Gapais (1979), Orientations préferentielles du quartz et orthogneissification progressive en régime cisaillant: L'example du cisaillement sud-armoricain, *Bull. Mineral.*, *102*, 265–272.
Bigi, G., A. Castellarin, M. Coli, G. V. Dal Piaz, R. Sartori, P. Scandone, and G. B. Vai (1990), Structural model of Italy, sheet 1, Cons. Naz. delle Ric., Progetto Finalizzato Geodin., SELCA, Florence, Italy.
Boullier, A. M., and Y. Gueguen (1975), SP mylonites: Origin of some mylonites by superplastic flow, *Contrib. Mineral. Petrol*, *50*, 93–104.
Brace, W. F., and D. L. Kohlstedt (1980), Limits on lithospheric stress imposed by laboratory experiments, *J. Geophys. Res.*, *85*, 6248–6252.
Carter, N. L., and S. H. Kirby (1978), Transient creep and semibrittle behavior of crystalline rocks, *Pure Appl. Geophys.*, *116*, 807–839.
Chester, F. M. (1995), A rheologic model for wet crust applied to strike-slip faults, *J. Geophys. Res.*, *100*, 13,033–13,044.
Christensen, J. N., J. Selverstone, J. L. Rosenfeld, and D. J. DePaolo (1994), Correlation by Rb-Sr geochronology of garnet growth histories from different structural levels within the Tauern Window, Eastern Alps, *Contrib. Mineral. Petrol.*, *118*, 1–12.
Cliff, R. A., G. T. R. Droop, and D. C. Rex (1985), Alpine metamorphism in the southeast Tauern Window, Austria: 2. Rates of heating, cooling and uplift, *J. Metamorph. Geol.*, *3*, 403–416.
Dunlap, W. J. (2000), Nature's diffusion experiment: The cooling-rate cooling-age correlation, *Geology*, *28*, 139–142.
Ellis, S., and B. Stöckhert (2004), Elevated stresses and creep rates beneath the brittle-ductile transition caused by seismic faulting in the upper crust, *J. Geophys. Res.*, *109*, B05407, doi:10.1029/2003JB002744.
Evans, J. P. (1988), Deformation mechanisms in granitic rocks at shallow crustal levels, *J. Structural Geology*, *10*, 437–443.
Frisch, W., J. Kuhlemann, I. Dunkl, and A. Brügel (1998), Palinspastic reconstruction and topographic evolution of the Eastern Alps during the late Tertiary tectonic extrusion, *Tectonophysics*, *297*, 1–15.
Gueydan, F., Y. M. Leroy, L. Jolivet, and P. Agard (2003), Analysis of continental midcrustal strain localization induced by microfracturing and reaction-softening, *J. Geophys. Res.*, *108*(B2), 2064, doi:10.1029/2001JB000611.
Hacker, B. R. (1997), Diagenesis and the fault-valve seismicity of crustal faults, *J. Geophys. Res.*, *102*, 24,459–24,467.
Hacker, B. R., and J. M. Christie (1990), Brittle/ductile and plastic/cataclastic transitions in experimentally deformed and metamorphosed amphibolite, in *The Brittle-Ductile Transition in Rocks*, *Geophys. Monogr. Ser.*, vol. 56, edited by A. G. Duba et al., 127–147, AGU, Washington, D. C.
Hippertt, J. F. (1998), Breakdown of feldspar, volume gain and lateral mass transfer during mylonitization of granitoid in a low metamorphic grade shear zone, *J. Struct. Geol.*, *20*, 175–193.
Hirth, G., and J. Tullis (1992), Dislocation creep regimes in quartz aggregates, *J. Struct. Geol.*, *14*, 145–159.
Hobbs, B. E., A. Ord, and C. Teyssier (1986), Earthquakes in the ductile regime?, *Pure Appl. Geophys.*, *124*(1–2), 309–336.
Imber, J., R. E. Holdsworth, C. A. Butler, and R. A. Strachan (2001), A reapparaisal of the Sibson-Scholz fault zone model: The nature of the frictional to viscous ("brittle-ductile") transition along a long-lived, crustal-scale fault, Outer Hebrides, Scotland, *Tectonics*, *20*, 601–624.
Ingles, J., C. Lamouroux, J.-C. Soula, N. Guerrero, and P. Debat (1999), Nucleation of ductile shear zones in a granodiorite under greenschist facies conditions, Néovielle massif, Pyrenees, France, *J. Struct. Geol.*, *21*, 555–576.
Ito, K. (1999), Seismogenic layer, reflective lower crust, surface heat flow and large inland earthquakes, *Tectonophysics*, *306*, 423–433.
Jackson, J. A., H. Austrheim, D. McKenzie, and K. Priestley (2004), Metastability, mechanical strength, and the support of mountain belts, *Geology*, *32*(7), 625–628, doi:10.1130/G20397.1.
Janecke, S. U., and J. P. Evans (1988), Feldspar-influenced rock rheologies, *Geology*, *16*, 1064–1067.
Kupferschmied, M. P. (1994), Geologische Untersuchungen im Tauernfenster zwischen Hollersbach und Krimmler Achental, *Muench. Geol.*, *12*, 1–160.
Lin, A., S. Maruyama, A. Stallard, K. Michibayashi, A. Camacho, and K. Kano (2005), Propagation of seismic slip from brittle to ductile crust: Evidence from pseudotachylyte of the Woodroffe thrust, central Australia, *Tectonophysics*, *402*, 21–35.
Linzer, H. G., K. Decker, H. Peresson, R. Dell'Mour, and W. Frisch (2002), Balancing orogenic float of the eastern Alps, *Tectonophysics*, *354*, 211–237.
Lloyd, G. E., A. B. Farmer, and D. Mainprice (1997), Misorientation analysis and the formation and orientation of subgrain and grain boundaries, *Tectonophysics*, *279*, 55–78.
Meissner, R., and J. Strehlau (1982), Limits of stresses in continental crusts and their relationship to the depth-frequency distribution of shallow earthquakes, *Tectonics*, *1*, 73–89.
Mogi, K. (1974), On the pressure dependence of strength of rocks and the Coulomb fracture criterion, *Tectonophysics*, *21*, 273–285.
Oxburgh, E. R., R. S. J. Lambert, H. Baadsgaard, and J. G. Simons (1966), Potassium-argon age studies across the south-east margin of the Tauern window, the eastern Alps, *Verh. Geol. Bundesanst.*, *BA*, 17–33.
Passchier, C. W. (1982), Pseudotachylyte and the development of ultramylonite bands in the Saint-Barthelemy Massif, French Pyrenees, *J. Struct. Geol.*, *4*(1), 69–79.
Peresson, H., and K. Decker (1997a), Far-field effects of late Miocene subduction in the Eastern Carpatians: E-W compression and inversion of structures in the Alpine-Carpatian-Pannonian region, *Tectonics*, *16*, 38–56.
Peresson, H., and K. Decker (1997b), The Tertiary dynamics of the northern Eastern Alps (Austria): Changing paleostresses in a collisional plate boundary, *Tectonophysics*, *272*, 125–157.
Petit, J. P. (1987), Criteria for the sense of movement on fault surfaces in brittle rocks, *J. Struct. Geol.*, *9*, 597–608.
Ramsay, J. G., and M. I. Huber (1983), *The Techniques of Modern Structural Geology.* vol. 1, *Strain Analysis*, Academic, London.
Ratschbacher, L., W. Frisch, H.-G. Linzer, and O. Merle (1991a), Lateral extrusion in the eastern Alps: 2. Structural analysis, *Tectonics*, *10*, 257–271.
Ratschbacher, L., O. Merle, P. Davy, and P. Cobbold (1991b), Lateral extrusion in the eastern Alps: 1. Boundary conditions and experiments scaled for gravity, *Tectonics*, *10*, 245–256.
Rosenberg, C. L., J. P. Brun, and D. Gapais (2004), Indentation model of the Eastern Alps and the origin of the Tauern Window, *Geology*, *32*, 997–1000.
Rosenberg, C. L., S. Schneider, and J. Babist (2007), The western termination of the SEMP fault (eastern Alps) and its bearing on the exhumation of the Tauern Window, in *Tectonic Aspects of the Alpine-Carpathian-Dinaride System*, *Geol. Soc. Spec. Publ.*, in press.
Ruina, A. L. (1983), Slip instability and state variable friction laws, *J. Geophys. Res.*, *88*, 10,359–10,370.
Rutter, E. H. (1986), On the nomenclature of mode of failure transitions in rocks, *Tectonophysics*, *122*(3–4), 381–387.
Rutter, E. H., M. Casey, and L. Burlini (1994), Preferred crystallographic orientation development during plastic and superplastic flow of calcite rocks, *J. Struct. Geol*, *16*, 1431–1447.
Schmid, S. M., B. Fügenschuh, E. Kissling, and R. Schuster (2004), Tectonic map and overall architecture of the Alpine orogen, *Eclogae Geol. Helv.*, *97*, 93–117.
Scholz, C. H. (1988), The brittle-plastic transition and the depth of seismic faulting, *Geol. Rundsch.*, *77*, 319–328.
Scholz, C. H. (2002), *The Mechanics of Earthquakes and Faulting*, 471 pp., Cambridge Univ. Press, New York.
Selverstone, J., F. S. Spear, G. Franz, and G. Morteani (1984), High-pressure metamorphism in the SW Tauern Window, Austria: P-T paths from hornblende-kyanite-staurolite schists, *J. Petrol.*, *25*, 501–531.
Selverstone, J., G. Morteani, and J. M. Staude (1991), Fluid channelling during ductile shearing; transformation of granodiorite into aluminous schist in the Tauern Window, Eastern Alps, *J. Metamorph. Geol.*, *9*, 419–431.
Shigematsu, N., K. Fujimoto, T. Ohtani, and K. Goto (2004), Ductile fracture of fine grained plagioclase in the brittle-plastic transition regime: Implication for earthquake source nucleation, *Earth Planet. Sci. Lett.*, *222*(3–4), 1007–1022.

Shimamoto, T. (1989), The origin of S-C mylonites and a new fault-zone model, *J. Struct. Geol*, *11*, 51–64.

Sibson, R. (1980), Transient discontinuities in ductile shear zones, *J. Struct. Geol.*, *2*, 165–171.

Sibson, R. H. (1982), Fault zone models, heat flow, and the depth distribution of earthquakes in the continental crust of the United States, *Bull. Seismol. Soc. Am.*, *72*(1), 151–163.

Spear, F. S., and G. Franz (1986), P-T evolution of metasediments from the eclogite zone, South-Central Tauern Window, Austria, *Lithos*, *19*, 219–234.

Sperner, B., L. Ratschbacher, and R. Ott (1993), Fault-striae analysis; a Turbo Pascal program package for graphical presentation and reduced stress tensor calculation, *Comput. Geosci.*, *19*, 1361–1388.

Stipp, M., H. Stünitz, R. Heilbronner, and S. M. Schmid (2002), Dynamic recrystallization of quartz: Correlation between natural and experimental conditions, in *Deformation Mechanisms, Rheology and Tectonics: Current Status and Future Perspectives*, edited by S. D. Meer et al., *Geol. Soc. Spec. Publ.*, *200*, 171–190.

Thöni, M. (2006), Dating eclogite-facies metamorphism in the Eastern Alps—Approaches, results, interpretations: A review, *Mineral. Petrol.*, *88*, 123–148.

Tullis, J., and R. A. Yund (1977), Experimental deformation of dry Westerly Granite, *J. Geophys. Res.*, *82*(36), 5705–5718.

Tullis, J., and R. A. Yund (1992), The brittle-ductile transition in feldspar aggregates: An experimental study, in *Fault Mechanics and Transport Properties of Rocks*, edited by B. Evans and T.-F. Wong, pp. 89–117, Academic, San Diego.

von Blanckenburg, F., I. M. Villa, H. Baur, G. Morteani, and R. H. Steiger (1989), Time calibration of a PT-path from the Western Tauern Window, Eastern Alps: The problem of closure temperature, *Contrib. Mineral. Petrol*, *101*, 1–11.

Wheeler, J., D. J. Prior, Z. Jiang, R. Spiess, and P. W. Trimby (2001), The petrological significance of misorientations between grains, *Contrib. Mineral. Petrol.*, *141*, 109–124.

White, J. C. (1996), Transient discontinuities revisited; pseudotachylyte, plastic instability and the influence of low pore fluid pressure on deformation processes in the mid-crust, *J. Struct. Geol.*, *18*(12), 1471–1486.

Wintsch, R. P., R. Christoffersen, and A. K. Kronenberg (1995), Fluid-rock reaction weakening of fault zones, *J. Geophys. Res.*, *100*, 13,021–13,032.

J. Cole, B. Hacker, and G. Seward, Earth Sciences, University of California, Santa Barbara, CA 93106-9630, USA. (hacker@geol.ucsb.edu)

J. Dolan and E. Frost, Earth Sciences, University of Southern California, Los Angeles, CA 90089-0740, USA.

W. Frank, CEAL Laboratory, Slovak Academy of Sciences, 81704 Bratislava, Slovakia.

L. Ratschbacher, Geowissenschaften, Technische Universität Bergakademie Freiberg, D-09599 Freiberg, Germany.